Supplemental Data

Jumpstarting the Cytochrome P450 Catalytic Cycle with a Hydrated Electron

Huriye Erdogan,[†2] An Vandemeulebroucke,[‡3] Thomas Nauser,[†] Patricia L. Bounds,[†4] and Willem H. Koppenol[†1]

[†]From the Institutes of Inorganic and [‡]Organic Chemistry, Department of Chemistry and Applied Biosciences, Swiss Federal Institute of Technology, CH-8093 Zurich, Switzerland.

[1]To whom correspondence should be addressed. E-mail: koppenol@inorg.chem.ethz.ch
[2]Current address: İlko Argem Biyoteknoloji Merkezi, Teknopark İstanbul, Sanayi Mah, Teknopark Bulvarı, No: 1/3. Blok, B Girişi, Kat: 3, 34906, Pendik / İstanbul, Turkey
[3]Current address; Roche Pharma Research and Early Development, Chemical Biology, F. Hoffmann-La Roche Ltd., Grenzacherstrasse 124, 065/210, 4070 Basel, Switzerland
[4]Current address: Foundation for Research on Information Technology in Society, CH-8004 Zurich, Switzerland
[5]Abbreviations used: CYP101Fe^{3+}, cytochrome P450cam; Cpd 0, Compound 0, or $[FeOOH]^{2+}$; Cpd 1, Compound 1, or $[FeO^{2+}por^{\bullet+}]$; Cpd 2, Compound 2, or $[FeO]^{2+}$; e^-_{aq}, hydrated electron; Gy, Gray.

Contents (listed in order of appearance in main text):

Formation of CYP101[FeO_2]$^{2+}$ (Fig. S1)

To validate pulse radiolysis as a technique to observe the postulated intermediates, we followed the formation of CYP101[FeO_2]$^{2+}$ by reducing CYP101Fe^{3+} with e^-_{aq} in the presence of O_2 at 4°C. We find that the rate constant for O_2 binding to CYP101Fe^{2+} from pseudo-first-order plots of k vs [O_2] at 418 nm determined by pulse radiolysis (Fig. S1a, k = 2.1 × 10^5 $M^{-1}s^{-1}$) is consistent with that determined by stopped-flow spectrophotometry (Fig. S1b, k = 2.4 × 10^5 $M^{-1}s^{-1}$). These rate constants are smaller by a factor of three than that reported by Peterson et al. (1). The binding of O_2 to Fe^{2+}-heme has been described by these authors as a monophasic reversible reaction with $k_{obs} = k_f[O_2] + k_r$, where k_f = 7.7 × 10^5 $M^{-1}s^{-1}$ and k_r = 1.06 s^{-1} at 4°C. We followed the method of these authors to demonstrate that CYP101[FeO_2]$^{2+}$ is formed and remains stable for 1 min at 4°C (Fig. S1c).

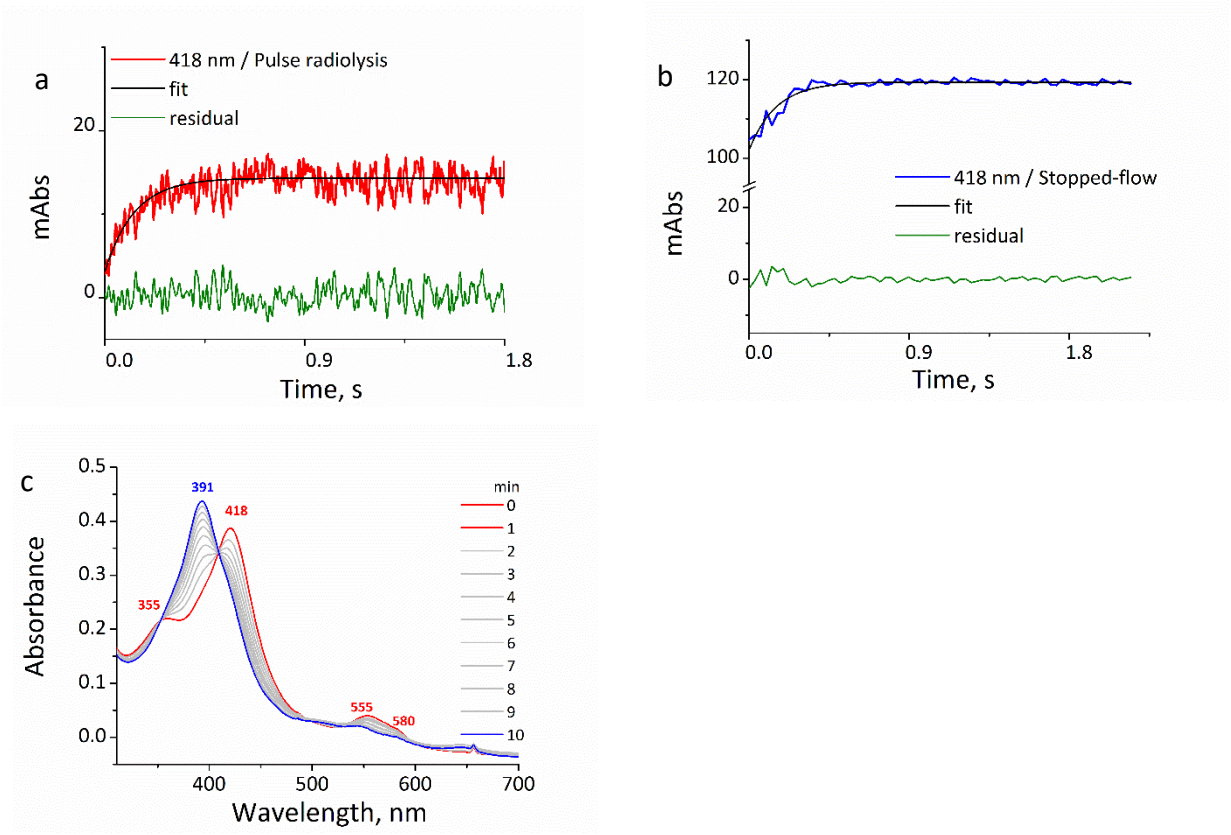

Figure S1. Formation of CYP101[FeO_2]$^{2+}$ a) by pulse radiolysis: a solution of 1 µM of CYP101Fe^{3+} was reduced with [e^-_{aq}] = 22 µM corresponding to a dose of 80 Gy, in the presence of excess O_2 at 32 µM (the nominal amount of O_2 added, 50 µM, is lowered by reaction with e^-_{aq} to form $O_2^{\bullet-}$ see Fig. S2); the rate constant for formation of CYP101[FeO_2^{2+}]: 2.1 × 10^5 M^{-1} s^{-1}; b) by stopped-flow spectroscopy: a solution of 4 µM CYP101Fe^{2+} with 8 µM camphor was reduced anaerobically with $S_2O_4^{2-}$ and mixed with buffer containing 50 µM O_2 at 4°C; rate constant for formation of CYP101[FeO_2]$^{2+}$: 2.4 × 10^5 M^{-1} s^{-1}. c) UV-VIS studies: a N_2-saturated solution 5.5 µM in CYP101Fe^{3+} was reduced by addition of $Na_2S_2O_4$ to 10 µM in the presence of 11 µM camphor, transferred to a quartz cuvette, and flushed with O_2 for 30 s at 7.0°C; absorbance spectra of CYP101[FeO_2]$^{2+}$ (—) decaying (—) to CYP101Fe^{3+} (—).

Simulated changes in O_2 concentration during pulse radiolysis (Fig. S2)

It is important to note that the O_2 concentration, 50 µM before the pulse, decreases because of the rapid competing reduction of O_2 by e^-_{aq}. We used the Chemical Kinetics Simulator (IBM) and published rate constants (2) to simulate the reactions shown in Table S1 and determined that the concentration of O_2 available to $CYP101Fe^{2+}$ is 32 µM.

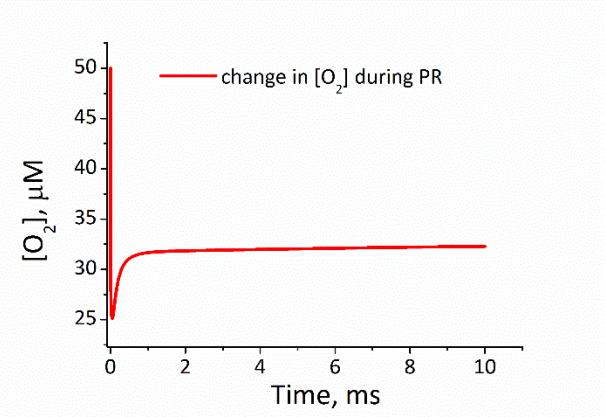

Figure S2. Simulated change in the concentration of 50 µM O_2 during pulse irradiation. The kinetics simulation shows that 32 µM O_2 is available to bind to $CYP101Fe^{2+}$; 32 µM is the concentration of O_2 used to calculate the rate constant for the formation of $CYP101[FeO_2]^{2+}$. The reactions in Table S1 (2) were used to calculate the remaining O_2 concentration. Reactions that involve the protein were not included in this simulation.

Catalytic activity of CYP101 before and after pulse radiolysis (Fig. S3)

As a measure of the catalytic activity of CYP101, we determined the rate of NADH oxidation at 387 nm (3). The reaction mixture typically contained 0.5 μM putidaredoxin reductase, 5 μM putidaredoxin, 0.1 μM CYP101, 2 mM camphor, 1 mM NADH, and 1 mM *t*-BuOH, in 10 mM potassium phosphate buffer, pH 7.4; the determination was carried out at room temperature. Reactions were started by adding NADH ($\varepsilon_{387} = 0.622 \times 10^3\ M^{-1}\ cm^{-1}$). Similar catalytic activity in terms of NADH oxidation was found before ($k_{obs\_activity} = (3.8 \pm 0.2) \times 10^2\ min^{-1}$) and after ($k_{obs\_activity} = (3.7 \pm 0.3) \times 10^2\ min^{-1}$) pulse radiolysis, which indicates that the irradiation does not damage the catalytic activity of the protein.

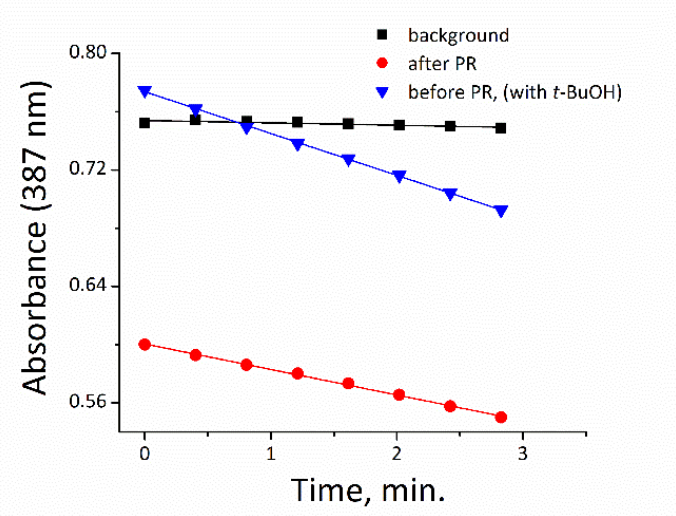

Figure S3. Catalytic activity of CYP101. The rate of NADH oxidation at 387 nm (3), before and after pulse radiolysis in the presence of 1 mM *t*-BuOH, showing that the reaction rate, $k_{obs\_activity} = 3.7 \pm 0.3\ 10^2\ min^{-1}$, is unchanged by pulse radiolysis.

Kinetics in deuterated solvent (Fig. S4)

To determine whether there is a solvent isotope effect on the lifetimes of intermediates, we performed the pulse radiolysis experiments in D_2O with deuterated potassium phosphate buffer. Comparison of the decay at 440 nm in D_2O with that in H_2O indicates that there is a kinetic isotope effect of ca. 2. In contrast to data acquired in normal aqueous solution, the initial absorbance increase is lower; even when the different radiochemical yields (G-values) in both solvents (4) are taken into account. Nevertheless, an analysis of the kinetics can be performed.

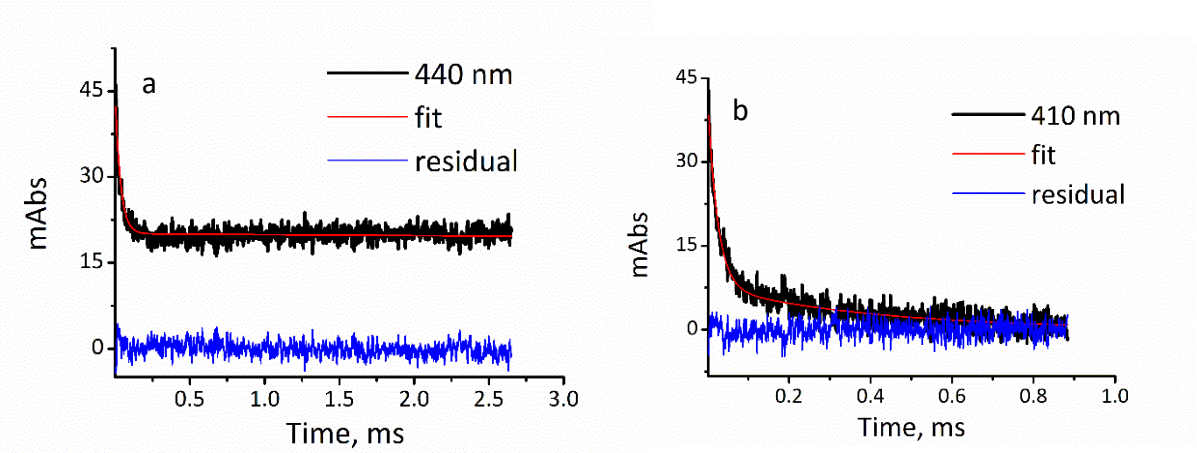

Figure S4. Reaction of e_{aq}^- with CYP101[FeO_2]$^{2+}$ at 4.0°C in deuterated potassium phosphate buffer. 5 µM CYP101Fe^{2+} and 10 µM camphor in D_2O were mixed 1 : 1with 100 µM O_2 and 2 mM *t*-BuOD in D_2-potassium phosphate, at pH 7.4, from two gas-tight syringes; the mixture was irradiated at 80 Gy, ([e_{aq}^-] = 22 µM) within 30 s after mixing. a) The decay of the absorbance at 440 nm (—) and the fit to a single rate constant k_{440nm} (D_2O) = 3.9 × 10^4 s^{-1} (—). b) The decay of the absorbance at 410 nm (—) and the fit to two rate constants: $k_{410nm\text{-}I}$ (D_2O) = 4.0 × 10^4 s^{-1} and $k_{410nm\text{-}II}$ (D_2O) = 2.3 × 10^3 s^{-1} (—).

Simulation of concentrations of reaction species during pulse radiolysis reaction (Fig. S5)

We used the Chemical Kinetics Simulator (IBM) and published rate constants listed in Table S1 to simulate the concentrations of the reaction species, including the primary oxidant, CYP101[FeOOH]$^{2+}$, during pulse radiolysis.

Hydrated electrons react at a diffusion-controlled rate with both O_2 and proteins (see Table S1). In the presence of O_2, the yield of reduced protein per e^-_{aq} is low (Fig. S5); however, the relatively low yield is observed only for the reduction of the enzyme; the remainder of the cycle operates quantitatively. The rate constant for the reaction of e^-_{aq} with the entire protein, which reflects reactions with both the heme and the protein parts of CYP101, is 3×10^{10} $M^{-1}s^{-1}$ (5,6). In the case of CYP101, the heme is buried and the surrounding aromatic residues likely act as a sink for e^-_{aq} (7,8), i.e., the reduction of the heme by e^-_{aq} is not quantitative, in agreement with the literature (5,6). We estimate the yield of CYP101Fe^{2+} from the reaction of e_{aq}^- with CYP101Fe^{3+}, reaction 2, and assume this yield to also apply to the reaction of e^-_{aq} with CYP101[FeO$_2$]$^{2+}$, reaction 3.

In the absence of O_2, the reaction of e^-_{aq} and H$^\bullet$ with amino acids leads to formation of adducts of e^-_{aq} and H$^\bullet$ with amino acids, which subsequently reduce CYP101Fe^{3+} by tunneling or hopping. With O_2 present, the majority of e^-_{aq} and H$^\bullet$ are scavenged to form $O_2^{\bullet-}$. Any e^-_{aq} or H$^\bullet$ adducts of amino acids would also be scavenged by O_2. Thus, the yield of reduction of the heme is lowered in experiments performed with O_2 present.

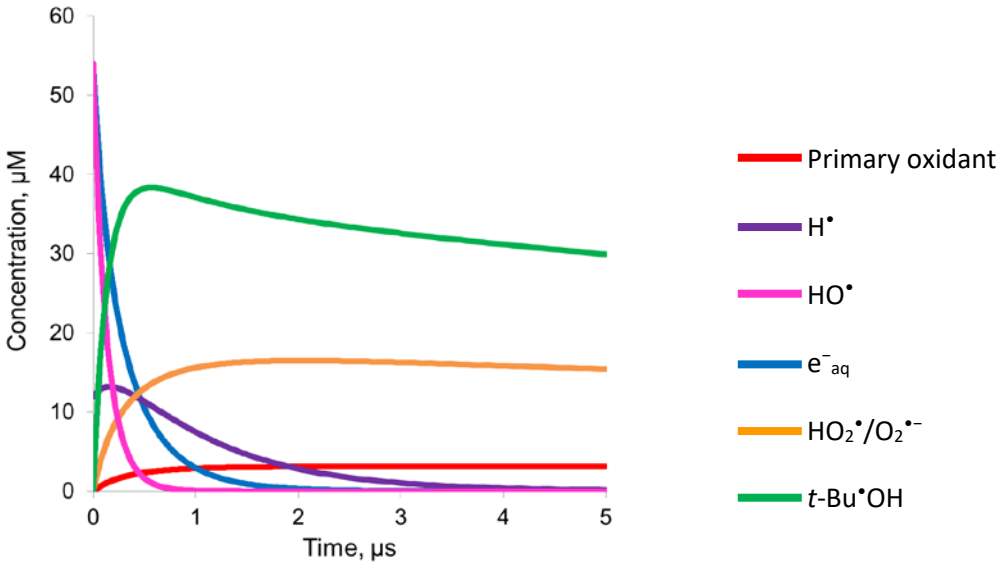

Figure S5. Simulation of the concentrations of several species formed during the reaction of CYP101[FeO$_2$]$^{2+}$ with e_{aq}^-. The simulation with the conditions of the product analysis experiment, i.e., 50 µM CYP101[FeO$_2$]$^{2+}$ reacting with 54 µM e_{aq}^- from a pulse of 200 Gy and with k_3 set at 3.9×10^9 M^{-1} s^{-1} is shown. Other values of k_3 ($3.1 - 4.5 \times 10^9$ M^{-1} s^{-1}, not shown) were also simulated. Simulations indicate a maximum yield of enzymatic primary oxidant, and, hence, of 5-hydroxycamphor, of 3.1 ± 0.6 µM.

Formation of 5-ketocamphor (Fig. S6)

We used GC-MS to analyze the formation of 5-ketocamphor after pulse radiolysis of CYP101 with camphor present.

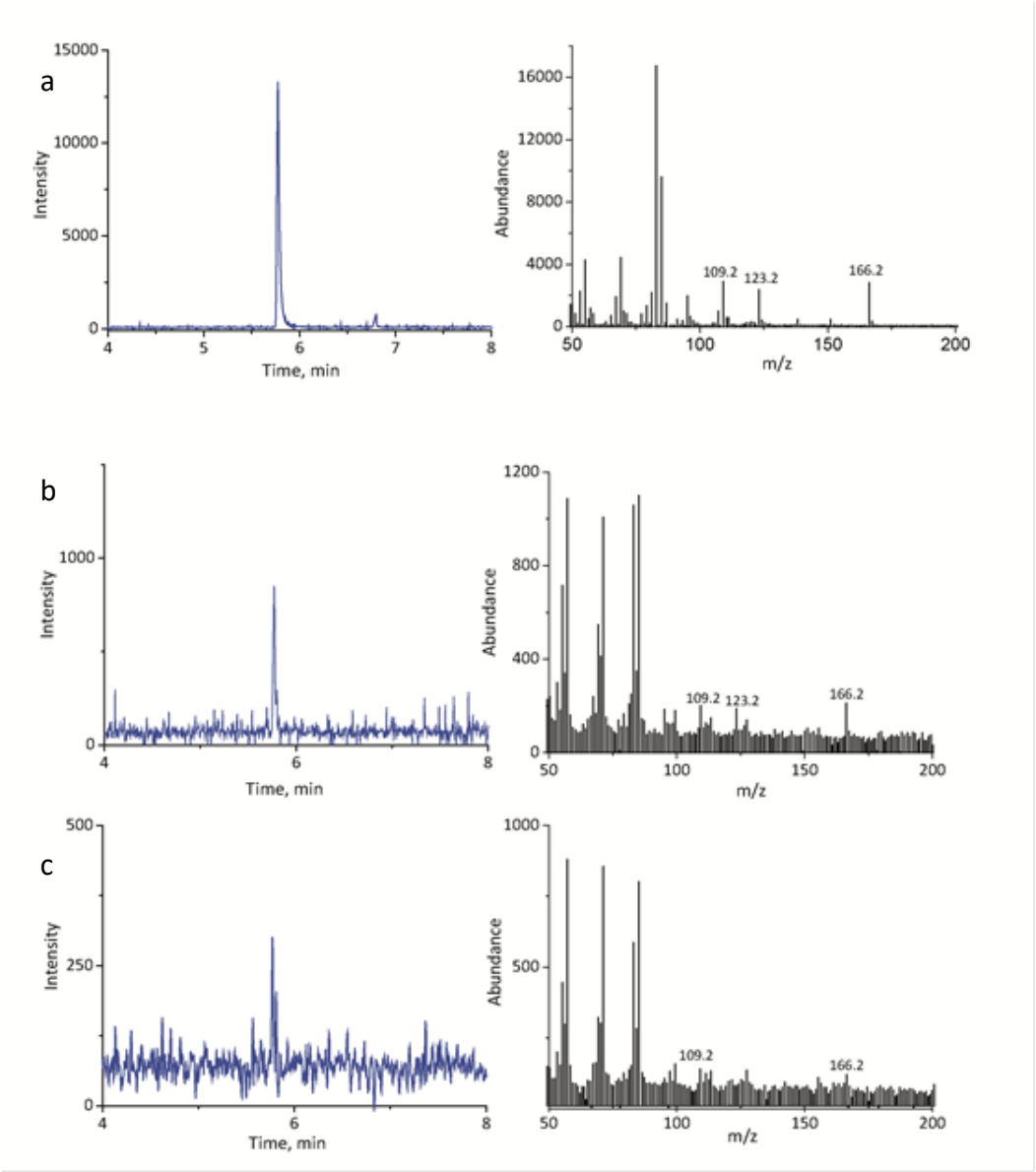

Figure S6. Elution profiles for *m/z* = 166 with corresponding mass spectra. a) 2 mM 5-hydroxycamphor mixed with 2 mM H_2O_2 in the presence of 20 µM CYP101; b) 75 µM of CYP101Fe^{2+} in the absence of camphor in buffer containing 100 µM O_2, irradiated with a dose of 200 Gy, collected in a sample tube containing 100 µM 5-hydroxycamphor; and c) 50 µM CYP101Fe^{3+} with 100 µM 5-hydroxycamphor in buffer containing 50 µM O_2, irradiated with a dose of 200 Gy, collected in a tube containing buffer.

Expression and purification of CYP101 (Fig. S7)

CYP101 was produced and purified as previously described (9), with slight modifications (3,10). *E. coli* BL21 cells were transformed with the pMG211 expression vector in a two-step growth procedure: the growth medium was supplemented with 100 µg/mL ampicilin, 0.5% glucose, 1% *w*/*w* vitamin solution, trace elements (concentrations: 2 mM $MgSO_4$•$7H_2O$, 0.1 mM $CaCl_2$ and $FeCl_2$, 50 µM H_3BO_4, 0.2 µM $CoCl_2$•$6H_2O$, 1 µM $CuSO_4$•$5H_2O$, 1 µM $MnCl_2$•$4H_2O$, 1 nM Na_2MoO_4, 1 nM $NiCl_2$•$6H_2O$, and 2 µM $ZnSO_4$). The heme precursor δ-aminolevulinic acid was added gradually to a concentration of 2.5 mM. Purification was carried out at 4°C**.** Cell cultures of 500 mL typically yielded 55–60 mg of protein of high purity – based on the published extinction coefficient, 102 $mM^{-1}\,cm^{-1}$ at 391 nm (11) and the ratio A_{392}/A_{280} = 1.62 (12). X-band continuous wave-EPR at 8 K was used to assign the g_x, g_y, and g_z values of 1.90, 2.25, 2.45 to low-spin, and of 1.78, 3.97, 7.73 to high-spin CYP101Fe^{3+} and to demonstrate that CYP101 with camphor bound exists as a 60:40 mixture of high and low spin forms at low temperatures as expected (13,14).

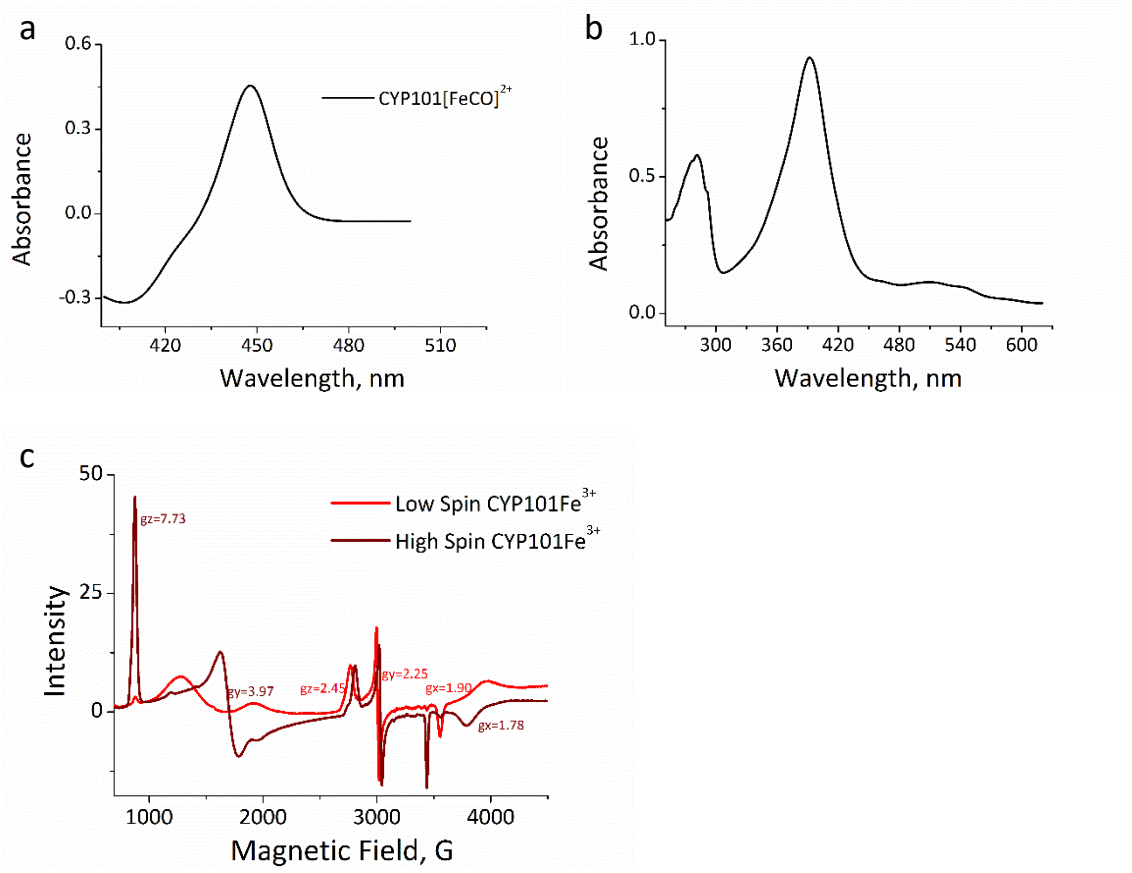

Figure S7. Quality of the expressed and purified CYP101. a) UV-VIS spectrum for CO binding experiment; b) UV-VIS spectrum of purified protein; c) X-band CW-EPR spectrum taken at 8 K in the absence of camphor for the low-spin form, CYP101Fe^{3+} (—) and in the presence of camphor for the high spin-form, CYP101Fe^{3+} (—).

Rate constants used to simulate pulse radiolysis reaction (Table S1)

Table S1

Rate constants of reactions used to simulate changes in concentrations of reactive species during pulse irradiation (see Figs. S2 and S5)

Reaction number	Reaction	Rate constant
1[a, b]	$2\ e^-_{aq} + 2\ H^+ \rightarrow H_2$	$5 \times 10^9\ M^{-1}s^{-1}$
2[a,b]	$e^-_{aq} + H^\bullet + H^+ \rightarrow H_2$	$2.5 \times 10^{10}\ M^{-1}s^{-1}$
3[a, b]	$e^-_{aq} + HO^\bullet + H^+ \rightarrow H_2O$	$3 \times 10^{10}\ M^{-1}s^{-1}$
4[a, b]	$2\ H^\bullet \rightarrow H_2$	$7.8 \times 10^9\ M^{-1}s^{-1}$
5[a, b]	$H^\bullet + HO^\bullet \rightarrow H_2O$	$7 \times 10^9\ M^{-1}s^{-1}$
6[a, b]	$2\ HO^\bullet \rightarrow H_2O_2$	$5.5 \times 10^9\ M^{-1}s^{-1}$
7[a, b]	$HO_2^\bullet + HO^\bullet \rightarrow O_2 + H_2O$	$6.6 \times 10^9\ M^{-1}s^{-1}$
8[a ,b]	$HO^\bullet$ + *t*-BuOH → *t*-Bu$^\bullet$OH + H_2O	$6 \times 10^8\ M^{-1}s^{-1}$
9[a, b]	$e^-_{aq} + O_2 + H^+ \rightarrow HO_2^\bullet$	$2 \times 10^{10}\ M^{-1}s^{-1}$ [c]
10[a,b]	$H^\bullet + O_2 \rightarrow HO_2^\bullet$	$2.1 \times 10^{10}\ M^{-1}s^{-1}$
11[a]	O_2 + *t*-Bu$^\bullet$OH → *t*-BuOO$^\bullet$ + $HO^\bullet$	$1 \times 10^9\ M^{-1}s^{-1}$
12[a]	*t*-BuOO$^\bullet$ + $HO_2^\bullet \rightarrow O_2$ + *t*-BuOOH	$1 \times 10^9\ M^{-1}s^{-1}$
13[a]	2 *t*-BuOO$^\bullet$ → + *t*-BuOO*t*-Bu + O_2	$1 \times 10^8\ M^{-1}s^{-1}$
14[a, b]	$2\ HO_2^\bullet \rightarrow O_2 + H_2O_2$	$8 \times 10^6\ M^{-1}s^{-1}$ [d]
15[b]	e^-_{aq} + $CYP101[FeO_2]^{2+}$ → primary oxidant	$4 \times 10^9\ M^{-1}s^{-1}$ [e]
16[b]	$e^-_{aq} + H_2PO_4 \rightarrow H^\bullet + HPO_4^-$	$2 \times 10^8\ M^{-1}s^{-1}$
17[b]	$e^-_{aq} + HO_2^\bullet + H^+ \rightarrow H_2O_2$	$1.3 \times 10^{10}\ M^{-1}s^{-1}$
18[b]	$H^\bullet + HO_2^\bullet \rightarrow H_2O_2$	$2 \times 10^{10}\ M^{-1}s^{-1}$
19[b]	e^-_{aq} + *t*-Bu$^\bullet$OH → *t*-BuO$^-$	$6 \times 10^9\ M^{-1}s^{-1}$
20[b]	$H^\bullet$ + *t*-Bu$^\bullet$OH → *t*-BuOH	$6 \times 10^9\ M^{-1}s^{-1}$

[a] Used to calculate changes in [O_2], Figure S2. [b] Used to calculate changes in the concentrations of other reactive species, Figure S5. [c] Includes the rate constant of e^-_{aq} with O_2. [d] Value at pH 7 for the reaction of $HO_2^\bullet$ with $O_2^{\bullet-}$ that includes the contribution of $HO_2^\bullet$ with $HO_2^\bullet$. [e] Taken to be equal to the rate constant for the reaction of e^-_{aq} with myoglobin (15).

Energetics of hydrogen abstraction from and hydroxylation of camphor

The energetics of the abstraction of a hydrogen atom from camphor, reaction S1, can be estimated:

$$\text{camphorH} + \text{Cpd 1} \rightarrow \text{camphor}^{\bullet} + \text{Cpd 2} \qquad \text{(S1)}$$

The relationship between the standard electrode potential and the bond dissociation enthalpy ($\Delta_{DBE}H°$) in the gas phase for abstraction of hydrogen from carbon 5 of camphor, CH, is:

$$\Delta_{DBE}H° = [2.11\ \text{V} + E°(\text{C}^{\bullet}, \text{H}^{+}/\text{CH})]96.5\ \text{kJ/mol V}^{-1} + 28.5\ \text{kJ/mol (16)} \qquad \text{(S2)}$$

in which $E°$ is an electrode potential, formerly a reduction potential. Equation S2 contains the most recently published value for $E°(\text{H}^{+}/\text{H}^{\bullet})$, –2.11 V (17). With the group additivity method of Benson (18-20) applied to C-4, C-5, and C-6 of camphor (18,21), we construct reaction S3 to calculate $\Delta_{BDE}H°$ = +397 kJ/mol, with $\Delta H°(\text{H}^{\bullet})$ = +218 kJ/mol (22), for H–C-5:

$$\text{C-5(2C,2H)} + \text{C-4(3C,H)} + \text{C-6(2C,2H)} \rightarrow \text{C}^{\bullet}\text{-5(2C,H)} + \text{C-4(C}^{\bullet}\text{,C,2H)} + \text{C-6(C}^{\bullet}\text{,C,2H)} + \text{H}^{\bullet} \qquad \text{(S3)}$$

The $\Delta_{BDE}H°$ of 397 kJ/mol calculated here for camphor agrees very well with that calculated by *in silico* methods (23). Equation S2 then yields $E°(\text{C}^{\bullet}, \text{H}^{+}/\text{RH})$ = +1.71 V and $E°'$ = +1.30 V at pH 7 for C-5 of camphor. Compared to the electrode potential of the Cpd 1/Cpd 2 couple of +1.35 V (24), we conclude that, within the error of these calculations, the abstraction of hydrogen from camphor, reaction S1, is essentially thermoneutral.

The rebound step, reaction S4:

$$\text{camphor}^{\bullet} + \text{Cpd 2} \rightarrow \text{CYP101Fe}^{3+} + \text{camphorOH} \qquad \text{(S4)}$$

can be divided into the two half-reactions S5 and S6:

$$\text{camphor}^{\bullet} + \text{H}_2\text{O} \rightarrow \text{camphorOH} + \text{H}^{+} + \text{e}^{-} \qquad \text{(S5)}$$

$$\text{CYP101FeOH}^{3+} + \text{H}^{+} + \text{e}^{-} \rightarrow \text{CYP101Fe}^{3+} + \text{H}_2\text{O} \qquad \text{(S6)}$$

The estimated value for $E°'$ of reaction S6 is +0.97 V (24). To estimate the $E°'$ of reaction S5, we use the isopropyl radical and 2-propanol as model compounds, as no experimental thermochemical data for the camphor radical and 5-hydroxycamphor are available. The Gibbs energies of formation for isopropanol, the isopropyl radical, and water of –173 (19), +142 (19), and –237 [(22)] kJ/mol, respectively, allow us to compute a $\Delta_{rxn}G°$ = +78 kJ/mol for reaction S7, the model compound equivalent of reaction S5:

$$CH_3CH^{\bullet}CH_3 + H_2O \rightarrow CH_3COHCH_3 + H^+ + e^- \quad \text{(S7)}$$

With the Nernst equation $\Delta G° = nF\Delta E°_{ox}$, in which $E°_{ox}$ is now an oxidation potential and F the Faraday constant, we calculate $E°_{ox}$ = +0.81 V and $E°'_{ox}$ = +1.22 V at pH 7 as estimates for the oxidation potential of reaction S5. The sum of reactions S5 and S6 is +2.19 V, thus $\Delta_{rebound}G°$ = –211 kJ/mol. To obtain values that reflect Gibbs energies in water, hydration energies of –13 kJ/mol and +16 kJ/mol are added to the Gibbs energies of formation of isopropanol and the isopropyl radical, respectively. The values of these corrections are estimated from comparisons of the Gibbs energies of formation of methane and methanol, and of ethane and ethanol, in the standard state and in water (22). Thus, the rebound step, reaction S4, is favorable by approximately 241 kJ/mol. Given the essentially thermoneutral H-abstraction, reactionS1, we write:

$$\text{Cpd 1} + \text{camphorH} \rightarrow \text{CYP101Fe}^{3+} + \text{camphorOH} \quad \text{(S8)}$$

with $\Delta_{rxn}G°'$ = –241 kJ/mol at pH 7.

References

1. Peterson, J. A., Ishimura, Y., and Griffin, B. W. (1972) *Pseudomonas putida* cytochrome P-450: Characterization of an oxygenated form of the hemoprotein. *Arch. Biochem. Biophys.* **149,** 197-208
2. NIST Chemical Kinetics Database, Standard Reference Database 17, Version 7.0, Release 1.4.3 http://kinetics.nist.gov/kinetics/index.jsp. National Institute of Standards and Technology (2009)
3. Aldag, C., Gromov, I. A., García-Rubio, I., von Koenig, K., Schlichting, I., Jaun, B., and Hilvert, D. (2009) Probing the role of the proximal heme ligand in cytochrome P450cam by recombinant incorporation of selenocysteine. *Proc. Natl. Acad. Sci. USA* **106,** 5481-5486
4. Chernovitz, A. C. and Jonah, C. D. (1988) Isotopic dependence of recombination kinetics in water. *J. Phys. Chem.* **92,** 5946-5950
5. Debey, P., Land, E. J., Santus, R., and Swallow, A. J. (1979) Electron transfer from pyridinyl radicals, hydrated electrons, carbon dioxide radical and superoxide radical to bacterial cytochrome P450. *Biochem. Biophys. Res. Commun.* **86,** 953-960
6. Hasinoff, B. B. (1985) Quantitative structure-activity relationships for the reaction of hydrated electrons with heme proteins. *Biochim. Biophys. Acta* **829,** 1-5
7. Braams, R. (1966) Rate constants of hydrated electron reactions with amino acids. *Radiat. Res.* **27,** 319-329
8. Getoff, N. (1992) Pulse radiolysis of aromatic amino acids - State of the art. *Amino Acids* **2,** 195-214
9. Shimoji, M., Yin, H., Higgins, L., and Jones, J. P. (1998) A functional bacterial/human cytochrome P450 chimera. *Biochemistry* **37,** 8848-8852
10. Vandemeulebroucke, A., Aldag, C., Stiebritz, M. T., Reiher, M., and Hilvert, D. (2015) Kinetic consequences of introducing a proximal selenocysteine ligand into cytochrome P450cam. *Biochemistry* **54,** 6692-6703
11. Guengerich, F. P., Martin, M. V., Sohl, C. D., and Cheng, Q. (2009) Measurement of cytochrome P450 and NADPH-cytochrome P450 reductase. *Nature Protocols* **4,** 1245-1251
12. Gunsalus, I. C. and Wagner, G. C. (1978) Bacterial P-450$_{cam}$ methylene monooxygenase components: Cytochrome *m*, putidaredoxin, and putidaredoxin reductase. In Fleischer, S. and Packer, L., editors. *Methods in Enzymology. Biomembranes - Part C: Biological Oxidations,* Academic Press, 166-188
13. Lipscomb, J. D. (1980) Electron paramagnetic resonance detectable states of cytochrome P450$_{cam}$. *Biochemistry* **19,** 3590-3599
14. Schünemann, V., Jung, C., Terner, J., Trautwein, A. X., and Weiss, R. (2002) Spectroscopic studies of peroxyacetic acid reaction intermediates of cytochrome P450cam and chloroperoxidase. *J. Inorg. Biochem.* **91,** 586-596
15. Wilting, J., Nauta, H., and Braams, R. (1971) The reaction rate constant of hydrated electron with some hemoproteins as a function of the pH. *FEBS Lett.* **16,** 147-151
16. Koppenol, W. H. (1990) Oxyradical reactions: From bond-dissociation energies to reduction potentials. *FEBS Lett.* **264,** 165-167
17. Armstrong, D. A., Huie, R. E., Koppenol, W. H., Lymar, S. V., Merényi, G., Neta, P., Ruscic, B., Stanbury, D. M., and Steenken, S. (2015) Standard electrode potentials involving radicals in aqueous solution: Inorganic radicals. *Pure Appl. Chem.* **87,** 1139-1150
18. Benson, S. W. (1976) *Thermochemical Kinetics*, 2 Ed., John Wiley & Sons, New York
19. Burke, S. M., Simmie, J. M., and Curran, H. J. (2015) Critical evaluation of thermochemical properties of C_1–C_4 species: Updated group-contributions to estimate thermochemical properties. *J. Phys. Chem. Ref. Data* **44,** 013101
20. Cohen, N. (1996) Revised group additivity values for enthalpies of formation (at 298 K) of carbon-hydrogen-oxygen compounds. *J. Phys. Chem. Ref. Data* **25,** 1411-1481
21. Bhattacharya, A. and Shivalkar, S. (2006) Re-tooling Benson's Group Additivity method for estimation of the enthalpy of formation of free radicals: C/H and C/H/O groups. *J. Chem. Eng. Data* **51,** 1169-1181

22. Wagman, D. D., Evans, W. H., Parker, V. B., Schumm, R. H., Halow, I., Bailey, S. M., Churney, K. L., and Nuttal, R. L. (1982) Selected values for inorganic and C_1 and C_2 organic substances in SI units. *J. Phys. Chem. Ref. Data* **11 (Suppl. 2),** 37-38
23. de Visser, S. P., Kumar, D., Cohen, S., Shacham, R., and Shaik, S. (2004) A predictive pattern of computed barriers for C-H hydroxylation by Compound I of cytochrome P450. *J. Am. Chem. Soc.* **126,** 8362-8363
24. Koppenol, W. H. (2007) Oxygen activation by cytochrome P450: A thermodynamic analysis. *J. Am. Chem. Soc.* **129,** 9686-9690